ORNL/TM-2008/167

Fracture Stress Data for SiC Layers in TRISO-Coated Fuel Particles

Thak Sang Byun, Jin Weon Kim, Ivan Dunbar, and John D. Hunn

September 22, 2008

Prepared for

Office of Nuclear Energy Science and Technology

Prepared by

OAK RIDGE NATIONAL LABORATORY
Oak Ridge, Tennessee 37831
managed by
UT-BATTELLE, LLC
for the
U.S. DEPARTMENT OF ENERGY
Under contract DE-AC05-00OR22725

Fracture Stress Data for SiC Layers in TRISO-Coated Fuel Particles

Thak Sang Byun, Jin Weon Kim*, Ivan Dunbar, and John D. Hunn
Materials Science and Technology Division, Oak Ridge National Laboratory, P. O. Box 2008, MS-6151, Oak Ridge, TN 37831
*Visiting scholar from the Chosun University in South Korea

Summary

A crush testing method for hemispherical shell specimens was developed based on the result of finite element (FE) analysis on stress distribution, and was applied to the evaluation of fracture strength for the chemical vapor deposited (CVD) SiC layers of tri-isotropic (TRISO) fuel particles. This report presents descriptions on the testing and evaluation procedures, SiC fracture data, and Weibull statistics parameters.

In the mechanical testing, hemispherical shell specimens of SiC layers removed from TRISO particles were diametrically loaded between a bottom base and a plunger with brass foil at its end. The fracture in the shells always initiates at the inner surface below the loading contact at the convex (outer) surface. Producing a highly uniform stress distribution under the loading contact area is necessary to accurately evaluate the fracture stress from the measured fracture load data by using an analytical solution. Finite element analysis confirms that a relatively soft metal (brass foil) inserted between the specimen's convex surface and plunger tip produced a highly uniform stress distribution under the contact area. Some conventional crust test methods without defining effective volume or area cause difficulties in interpretation of fracture strength data because a strong size effect exists in the fracture test results from miniature specimens. In this study a major improvement was made by using a simple experimental method to obtain the effective area.

Nine(9) sets of hemispherical shell specimens were prepared by grinding off 45~50% of the fuel spheres and burning off the carbon layers at 700 ºC to obtain free standing SiC. These sample sets were obtained from several relevant lots of coated fuel particles, which include AGR fuels, a German reference fuel, and other development fuels available at Oak Ridge National Laboratory. At least 30 specimens were tested at room temperature for each material and the fracture stress data were analyzed using Weibull statistics. The diameters of the loading-contact area were measured from the impression formed in the brass foil.

The size effect in strength is significant in the specimen size range tested. In this analysis, therefore, the local fracture stress (the fracture stress for the loaded volume only) was calculated from the measurements of fracture load and contact diameter. This was converted to the fracture stress for the full spherical shells, which can be used as reference data for design related analyses. The data listed in the tables are the fracture stress, contact diameters, local fracture stress, fracture stress for the full spherical shell, scale parameter, mean value and Weibull modulus for each data set.

The mean fracture stress varied with test material in the range of 330 – 650 MPa; the values for scale parameter were about 17% higher than the mean fracture stress. Among the test materials

B&W-93060 had the lowest fracture stress of about 330 MPa and LEU01-49T exhibited the highest strength at about 650 MPa. The Weibull modulus was in the range of 3.98 – 7.25; the LEU01-46T SiC showed the largest scatter in data and therefore the lowest modulus, 3.98.

The fracture stress data could not be well connected to the microstructural characteristics. This might be because the degrees of roughness at the inner surface, which is believed to be the key fracture controlling factor, were not significantly different for coatings while unknown parameters produced larger differences in the strength data.

1. FE Analysis

The purpose of the FE analysis is to prove the feasibility of a soft metal insertion as a measure of expanding the uniformly stressed area at the inside wall of the SiC shell specimen during crush testing. This enables the use of an analytical solution for stress distribution. The main reason for pursuing this crush test method regardless of some complexity in calculation was the future application at high temperature or in an environmental chamber.

Fig. 1 presents the FE model used in the simulations using the ABAQUS code. Considering the geometrical symmetry of the specimens, an axi-symmetric model employing a four-node bilinear axi-symmetric element with reduced integration (CAX4R) was used. SiC shell specimens were assumed to be fully elastic with Young's modulus of 450 GPa and Poisson ratio of 0.21. The loading plunger (jig) was assumed to be a ridged body and for the input data of the insert material (brass), the tensile stress-strain curve was used. A friction coefficient of 0.25 was used for all contact surfaces.

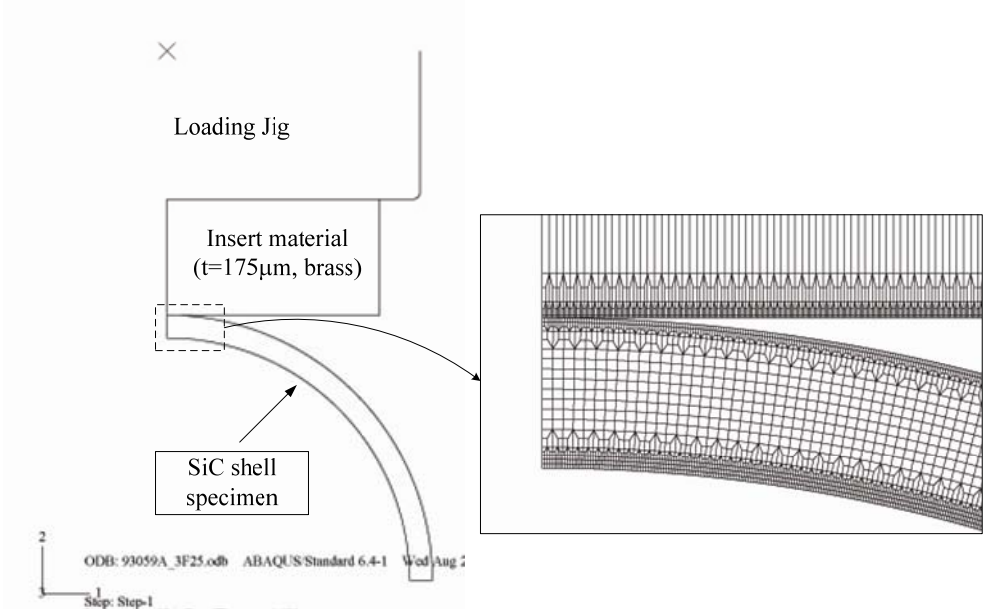

Fig. 1. Finite element model used in the analysis

Fig. 2 shows the distribution of maximum principal stress, which governs brittle fracture in elastic materials. As shown in Fig. 2, the highest value of maximum principal stress appeared at

the inner surface of the specimen below the loaded area (the contact area with the insert material). For the majority of the inner surface area just below the loading contact area, the stress variation is less than 10% of maximum stress, which justifies the use of the loading contact area for the effective area. Although the uniformly stressed area was slightly less than the loaded area at the outside wall of the specimen, the uniform area was larger than two times the specimen thickness in this example.

Having a reasonable size of uniformly stressed area is necessary because the analytical solution for stress calculation to be used in calculations is obtained for a concentrated load that is uniformly distributed over a defined contact area whose radius is larger than the thickness of the specimen [1]. It should be also considered that a high uniformity stress distribution can reduce the uncertainty in the evaluated fracture stress values. Based on the FE analysis result, we concluded that the use of a soft metal insert between the plunger and the specimen could produce adequate size and uniformity of the stressed and load-transferring area necessary for the use of the analytical solution.

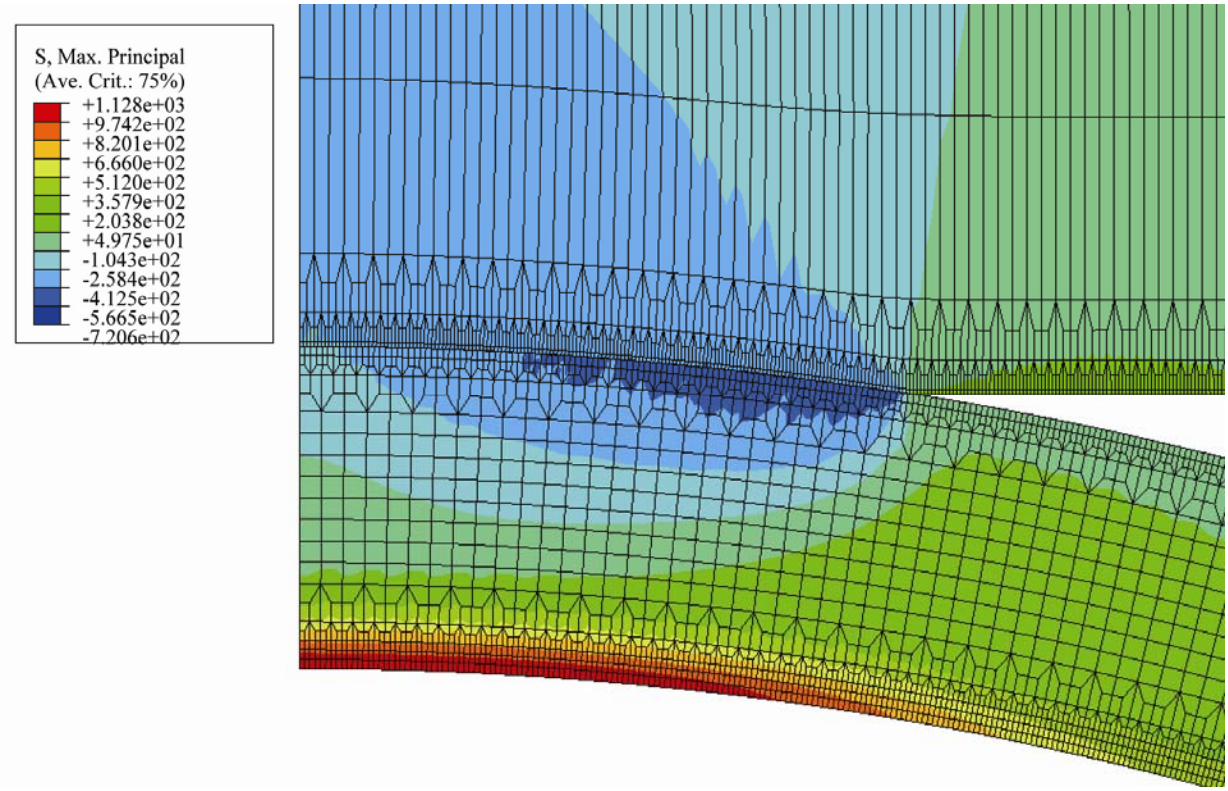

Fig. 2 Distribution of maximum principal stress at SiC shell specimen at a failure load

2. Experimental

Nine sets of particle samples were chosen, which included AGR fuels, a German reference fuel, and several other development batches. The particle samples used in this study are listed in

Table 1. They were chosen both for their relevance to the AGR program and to give a range of SiC grain sizes. The SiC layers have thicknesses in the range of 25 to 36 μm and outer diameters from 710 to 890 μm. These coatings also display variations in density, which originated from different conditions in the coating processes. The variation in density and thickness within a given sample set is indicated by the standard deviation in the measured mean given in Table 1.

Appendix A contains SEM images of polished cross sections for each SiC material listed in Table 1. These images show the relative grain size for the different samples. DUN500S-14B exhibited the smallest grain size. LEU01-49T and B&W-93060 ranked next in size, with B&W-93059, DUN500-7B and AGR-06 (German) just slightly larger in average grain size. LEU01-46T had noticeably larger grains in the outer portion, but would still be ranked as having an acceptably fine grain structure. DUN500-6B and AGR-10 (HRB-21) possessed relatively large grains, some extended up to half the total layer thickness. The finer grain structures also appeared to be more porous.

Particles were mounted on aluminum holders using a thermoplastic epoxy (Crystalbond). The particles were ground to near midplane with 9 μm diamond suspension on a cast iron disc (Struer's ALLEGRO). The exposed cross-sections were then polished using 3 μm diamond suspension on a silk disc (Struer's DAC). Kernels that had not already dropped out due to polishing to midplane were removed using adhesive tape. The particles were then removed from the epoxy by reheating the mount and washing off residual epoxy with acetone. Eight hours heating in air at 700°C was sufficient to burn off the carbon layers and yield free standing SiC hemispherical shells.

A screw-driven tensile machine with a 10 kg capacity load cell was used to load the specimens. Figure 3 illustrates the crush test setup, which shows a soft metal film inserted between the hemispherical shell specimen and the plunger (see Fig. 1). For each material, at least 30 specimens were tested at room temperature with a cross head speed of about 0.005 mm/sec. The machine was set to catch and display the maximum load, which was used as the fracture load. The diameters of the loading-contact area were measured from the impressions formed at the brass foil, and for each material the average value of the measurements was used in the calculation.

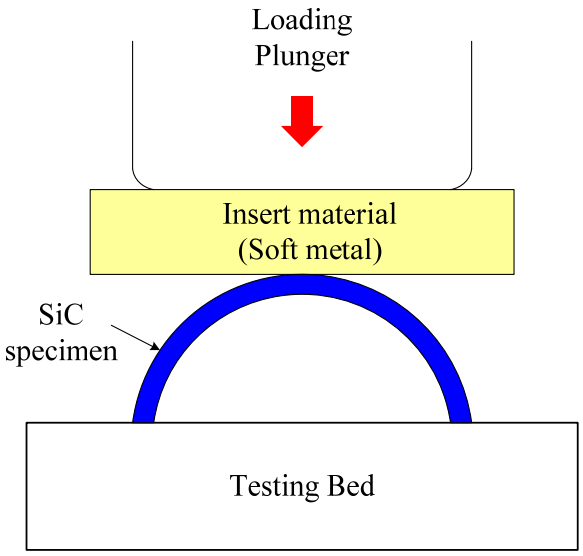

Figure 3. The crush test setup

3. Data analysis

3.1. Calculation of local fracture stress

When a partial spherical shell is diametrically loaded by an external load F concentrated on a small circular area of radius r_0, the stress components in the thin shells, the maximum membrane stress and bending stress, are given by [1]

$$\sigma_{menbrane} = -C_1 \frac{F\sqrt{1-\upsilon^2}}{t^2} \tag{1}$$

$$\sigma_{bending} = -C_2 \frac{F\sqrt{1+\upsilon}}{t^2} \tag{2}$$

where ν is Poisson ratio, t is the thickness of shell specimen, R is the outer diameter of the shell, and the coefficients C_1 and C_2 can be given by fitting equations:

$$C_1 = 0.2205 - 0.04\mu - 0.0115\mu^2 \tag{3}$$

and

$$C_2 = 1.2044\exp(-1.2703\mu); \tag{4}$$

$$\mu = r_0[12(1-\upsilon^2)/(R^2t^2)]^{1/4}. \tag{5}$$

Then, the maximum tensile stress which occurs at the inner surface of the shell is given by

$$\sigma_{\max} = \sigma_{membrane} + \sigma_{bending} \tag{6}$$

At fracture, this maximum stress becomes the fracture stress, which represents the local loading or the size of sampling. Since the fracture stress is dependent on the loaded volume or area and the size effect is significant in the range of the present specimen size, this local fracture stress is converted to the value for a full size spherical shell.

In the calculations we assumed that all dimensional measurements are the same for each set of specimens, ignoring variations in shape and size of specimen, in loading-contact area measurements, etc. Therefore, the Weibull moduli determined for data sets of fracture load and stress are the same and reflect the effects from such dimensional variations.

3.2. Calculation of Weibull parameters

It is well known that ceramic materials are notorious for their widely variable strength among seemingly identical specimens, and for the dependence of strength on the size and surface condition of the specimens [2-5]. Since the maximum tensile stress always occurs at the inner surface of the specimens and this surface has a large density of dimple-like features which might act as stress concentrators, the present statistical analysis assumes that failure initiates at the inner surface of the hemispherical shell specimens [7-9]. Thus the size effect is described based on the effective area. Using the Weibull's two-parameter distribution [4,5], the cumulative probability of failure P is presented by:

$$P = 1 - \exp[-S_E \left(\frac{\sigma_f}{\sigma_0} \right)^m], \tag{7}$$

where σ_f, m, σ_0, and S_E are the fracture stress, the Weibull modulus, the scale parameter, and the effective surface (or the load weighted surface), respectively. The Weibull modulus m, also called the shape parameter, represents the scatter in the fracture strength. The scale parameter σ_0, corresponding to the fracture stress with a failure probability of 63.2%, is closely related to the mean strength of the distribution. The term S_E represents the surface area of a hypothetical specimen subjected to a uniform stress over the whole surface area, which has the same probability of fracture as the test specimen stressed at σ_f. In this analysis the average value of the measured contact areas ($\pi \bar{r}_0^2$) was used for this parameter.

By taking the logarithm twice, Eq. (7) can be rewritten in a linear form:

$$\ln \ln \left(\frac{1}{1-P} \right) = m \cdot \ln \sigma_f + \ln \left(\frac{S_E}{\sigma_0^{\,m}} \right). \tag{8}$$

The Weibull modulus and scale parameter can be obtained from the slope and intercept terms in Eq. (8), respectively. Since the true value of P_i for each σ_i is not known, a prescribed

probability estimator has to be used as the value of P_i. There have been introduced several probability estimators and their merits have been investigated [10,11]. Among those probability estimators, it is shown that the probability estimator of Eq. (7) gives a conservative estimation, and therefore from the engineering point of view it should be the best choice in reliability predictions [10].

$$P_i = \frac{i}{N+1}, \tag{9}$$

where P_i is the probability of failure for the i th-ranked stress datum and N is the sample size.

3.3 Size effect and fracture stress for full spherical shell

The effective surface, which includes the effects from specimen geometry, multi-axial stress field, stress gradient, and chosen failure criterion on the reliability of a material, can be used to scale ceramic strengths from one component size to another or from one loading configuration to another [12]. Larger specimens or components are likely to be weaker because of their greater chance to have a larger and more severe flaw. For two specimens having different sizes or loading configurations, the ratio between their mean fracture strengths (or characteristic strengths) can be correlated with the ratio of the effective surface areas [7,8,12]:

$$\sigma_f^F = \left(\frac{S_E^L}{S_E^F}\right)^{1/m} \sigma_f^L = \left(\frac{\pi r_0^2}{4\pi(R-t)^2}\right)^{1/m} \sigma_f^L, \tag{10}$$

where σ_f^L and σ_f^F are the fracture stresses for partially loaded and full spherical shell specimens, respectively, S_E^L and S_E^F are the effective surfaces.

In the evaluation of the size effect the measured radius of indentation impression was used for the radius of effective area (r_0). Although these radii are different typically by several percent, as shown in the Fig. 2, one fracture stress converted from another is not significantly influenced by such a small difference because of the power 1/m.

4. Results and discussion

Table 2 summarizes the measured and calculated mean values for key parameters; the data for individual tests are in Tables 3 – 11. In each material the lowest fracture stress was often less than one half of the maximum value. The mean fracture stress varied with test material in the range of 330 – 650 MPa; the values for scale parameter were about 17% higher than the mean fracture stress. Among the test materials B&W-93060 had the lowest fracture stress of about 330 MPa and LEU01-49T the highest strength, about 650 MPa. These SiC strength values are similar to those obtained from the surrogate tubular specimens if size effect is taken into account; for example, the fracture stress obtained from the tubular SiC specimens with ~1 mm diameter and 0.1 mm wall thickness was about 300 MPa [7-9]. It is worth noting that, if we convert the mean

fracture stresses in Table 2 to those for the tubular specimens using Eq. (10), the values will be 25 - 45% lower depending on the specimen dimensions and Weibull modulus.

The Weibull modulus was in the range of 3.98 – 7.25. Except for LEU01-46T which showed the largest scatter in data or the lowest modulus (3.98), the test materials showed a modulus higher than 5. In determining these modulus values all dimensional variations among specimens were ignored, and therefore, these values are the same for the data sets for fracture load and fracture stress for each material.

It has been believed that the microstructural and geometrical parameters, such as grain size, surface roughness, porosity, and irregularities in thickness and diameter, determine the strength characteristics of SiC coatings. Although more focused and detailed investigation is needed for a final conclusion, the following paragraphs discuss the influences from those parameters:

(1) Although it is expected that a larger grain size induces lower fracture stresses because of higher stress concentrations at grain boundaries, the influence of grain size on the fracture stress is not clear in this study. Comparing the microstructures in appendix A, it is easily found that among the large grain materials are DUN500S-6B and ARG-10. However, their fracture stresses are not among the lowest although the fracture stress for DUN500S-6B is the third lowest one (Table 2). This indicates that the grain size is not a dominant factor determining the fracture process of a shell specimen.

(2) The roughness of the inner surface might be the controling factor for the initiation of fracture since the maximum stress always occurs at the inner surface where the dimple-like structure provides plenty of crack initiation sites. Note that the scaling using the effective area, Eq. (10), is based on the notion that the fracture initiates at the inner surface of the shell specimens. All pictures in Appendix A show high porosity near the inner surface of the coatings and SiC infiltrates into the inner pyrocarbon layer. The degree of roughness, however, is not discernable for those coatings. Therefore, seemingly the most influential microstructural property cannot explain the difference of the fracture stress data among the materials.

(3) The variances in the mean diameter and thickness, along with the shape irregularities in a specimen, should affect the strength result significantly. As listed in Table 1, however, we have very limited data for those parameters. Comparing the data for LEU01-46T and 49T, the specimen set with a larger standard deviation in thickness did not produce a larger scatter (or smaller Weibull modulus) in fracture stress data. It is believed that the deviation in the thickness is too small to produce a discernable effect in the strength results or its effect is compensated by other effects.

Finally, the size effect was significant: the scaling factor between the local fracture stress and the fracture stress for full size shell in the range 1.9 – 3.1. The fracture stress in the present specimen size range is considered not as a material property but as a property for a material plus a specific structure. Therefore, in the application of the data the effective area for the specific phenomenon should be evaluated and the fracture stress data provided be scaled up or down using the Eq. (10). For example, the fracture stress suggested for the full spherical shell should be scaled up when

one simulates the local fracture behavior at a sharp crack in a SiC coated fuel; while it should be scaled down if applied to a bulk material.

5. Conclusions

The crush test and evaluation method using a deformable metallic foil at the specimen-plunger contact was successfully applied to the evaluation of fracture stress for the hemispherical shell SiC specimens. The statistical characteristics of fracture stress are consistent with the earlier data for spherical shell or tubular specimens.

The statistical characteristics of fracture stress were not well explained by the varied microstructural characteristics of the materials studied. This might be because the degree of roughness at the inner surface, the main fracture controlling factor, was not discernable for different coatings while the fracture stress data evaluated were believed to result from the competition of effects from multiple parameters. A detailed investigation is needed on this issue, focusing on discerning the influences of individual parameters.

The size effect should be always considered in application of the data. The scale factor between the current shell specimen size and the stressed size in the new application can be calculated by Eq. (10) or other known equations. It is suggested that the dataset for use in design and assessment activities includes minimum components such as the fracture stress, effective area, and Weibull modulus.

Although the degree and number of variables in the samples studied was too great to draw firm conclusions as to the effects of individual properties on the strength of the SiC layers, this study did establish several facts. The test method was found to be self consistent and showed reasonably well controlled scatter between specimens in a given sample. The average SiC strength for shells typical of those found in TRISO particles was found to be in the range of 330-650 MPa.

References

[1] R.J. Roark, W.C. Young, “Formulas for Stress and Strain,” McGraw-Hill Book Co., Fifth Eds, New York, 1974.

[2] M. Jadaan, D.L. Shelleman, J.C. Conway, Jr., J.J. Mecholsky, Jr., and R.E. Tressler, “Prediction of the Strength of Ceramic Tubular Components: Part I - Analysis,” *JTEVA*, 19 (1991) 181-91.

[3] D.L. Shelleman, O.M. Jadaan, D.P. Butt, R.E. Tressler, J.R. Hellman, and J.J. Mecholsky, Jr., “High Temperature Tube Burst Test Apparatus,” *JTEVA*, 20 (1992) 275-84.

[4] ASTM Standard, “C1239-00 Standard Practice for Reporting Uniaxial Strength Data and Estimating Weibull Distribution Parameters for Advanced Ceramics,” American Society for Testing and Materials, Philadelphia, PA (2003).

[5] M.A. Madjoubi, C. Bousbaa, M. Hamidouche, and N. Bouaouadja, "Weibull Statistical Analysis of the Mechanical Strength of a Glass Eroded by Sand Blasting," *J. Eur. Ceram. Soc*., 19 (1999) 2957-62.
[6] T. Lin, A.G. Evans, and R.O. Ritchie, "A Statistical Model of Brittle Fracture by Transgranular Cleavage," *J Mech. Phys. Solids*, 21 (1986) 263-77.
[7] S.G. Hong, T.S. Byun, R.A. Lowden, L.L. Snead, Y. Katoh, "Evaluation of the Fracture Strength for SiC Layers in the TRISO-coated Fuel Particle," *J. of the Amer. Ceramics. Soc.* 90 (2007) 184-191.
[8] T. S. Byun, E. Lara-Curzio, L. L. Snead, Y. Katoh, "Miniaturized Fracture Stress Tests for Thin-Walled Tubular SiC Specimens," *J. of Nucl. Mater*. 367-370 (2007) 653-658.
[9] L. L. Snead, T. Nozawa, Y. Katoh, T. S. Byun, S. Kondo, D. A. Petti, "Handbook of SiC Properties for Fuel Performance Modeling," *J. of Nucl. Mater*. 371 (2007) 329-377.
[10] B. Bergman, "On the Estimation of the Weibull Modulus," *J. Mater. Sci. Lett*., **3** (1984) 689-92.
[11] A. Khalili and K. Kromp, "Statistical Properties of Weibull Estimators," *J. Mater. Sci*., **26**, 6741-52 (1991).
[12] D.G.S. Davies, "The Statistical Approach to Engineering Design in Ceramics," *Proc. Br. Ceram. Soc*., **22** (1973) 429-52.

Table 1. Dimensional and density data for hemispherical shell SiC specimens.

No.	Sample ID	Mean Thickness (μm)	Mean Outer Diameter (μm)	Mean Density (g/cc)	Remarks
1	DUN500S-14B	~25	~870	3.185±0.005	Mixed Ar/H SiC deposition at 1340°C, very fine grained and porous
2	DUN500S-6B	~30	~886	3.205±0.001	H only SiC deposition at 1510°C, large grain
3	DUN500S-7B	~35	~862	3.206±0.005	Mixed Ar/H SiC deposition at 1440°C, small grain
4	AGR-06	33.9±1.4	850	3.201±0.002	German reference fuel
5	AGR-10	26.8±0.6	718	3.206±0.002	US HRB-21 reference fuel
6	LEU01-46T	35.3±1.3	759	3.2075±0.0032	AGR-1 Baseline
7	LEU01-49T	35.9±2.1	756	3.2046±0.0010	AGR-1 Variant 3 (Ar-H mixed SiC deposition, finer grain structure at lower deposition temperature)
8	B&W-93059	34.3	~797	3.199	B&W AGR-2 Variant Qualification TRISO
9	B&W-93060	36.8	~813	3.195	B&W AGR-2 Baseline Qualification TRISO

Note: ± values give the measured standard deviation and indicate how much variation was observed for that property.

Table 2. Summary of fracture strength test result for hemispherical shell SiC specimens.

No.	Sample ID	Contact diameter, mm	Fracture load, N	Local fracture stress, MPa	**Weibull modulus**	**Fracture stress, MPa**	**Scale parameter, MPa**
1	DUN500S-14B	0.1179*	2.59	997.2	**6.61**	**449.8**	**539.2**
2	DUN500S-6B	0.1245	3.60	1050.5	**5.49**	**409.6**	**509.7**
3	DUN500S-7B	0.1421	5.32	1001.0	**7.25**	**514.7**	**602.0**
4	AGR-06	0.1472	5.84	1016.3	**6.22**	**475.4**	**567.8**
5	AGR-10	0.1131	4.20	1232.0	**6.40**	**570.7**	**645.1**
6	LEU01-46T	0.1533	11.36	1203.3	**3.98**	**399.1**	**490.4**
7	LEU01-49T	0.1405	8.64	1324.2	**6.35**	**646.5**	**737.1**
8	B&W-93059	0.1514	6.47	923.1	**6.58**	**463.9**	**537.4**
9	B&W-93060	0.1668	6.97	769.5	**5.15**	**329.9**	**398.0**

*Calculated from the load versus contact diameter data of the case no. 2.

Table 3. Fracture stress data for DUN500S-14B

[1] DUN500S-14B

No.	Thickness, mm	Diameter, mm	Contact diameter*, mm	Load, N	Local fracture stress, MPa	Size effect parameter	Weibull modulus (m)	Fracture stress, MPa	Scale parameter, MPa
1	0.025	0.435	0.1130	1.96	708.7	2.217	6.61	319.7	603.0
2	0.025	0.435	0.1426	2.00	723.1	2.217	6.61	326.2	552.7
3	0.025	0.435	0.1020	2.02	730.4	2.217	6.61	329.5	523.7
4	0.025	0.435	0.1927	2.10	759.3	2.217	6.61	342.5	519.9
5	0.025	0.435		2.32	838.8	2.217	6.61	378.4	553.9
6	0.025	0.435	0.1280	2.38	860.5	2.217	6.61	388.2	551.2
7	0.025	0.435	0.1296	2.42	875.0	2.217	6.61	394.7	546.0
8	0.025	0.435	0.1712	2.44	882.2	2.217	6.61	398.0	537.9
9	0.025	0.435	0.1207	2.44	882.2	2.217	6.61	398.0	526.8
10	0.025	0.435	0.1178	2.46	889.5	2.217	6.61	401.2	521.1
11	0.025	0.435	0.1629	2.54	918.4	2.217	6.61	414.3	528.6
12	0.025	0.435	0.1169	2.56	925.6	2.217	6.61	417.5	524.0
13	0.025	0.435		2.64	954.6	2.217	6.61	430.6	532.0
14	0.025	0.435		2.70	976.2	2.217	6.61	440.4	536.0
15	0.025	0.435	0.1089	2.80	1012.4	2.217	6.61	456.7	548.0
16	0.025	0.435	0.1588	2.82	1019.6	2.217	6.61	459.9	544.3
17	0.025	0.435	0.1458	2.82	1019.6	2.217	6.61	459.9	537.0
18	0.025	0.435	0.1816	2.86	1034.1	2.217	6.61	466.5	537.5
19	0.025	0.435		2.86	1034.1	2.217	6.61	466.5	530.6
20	0.025	0.435		2.90	1048.6	2.217	6.61	473.0	531.1
21	0.025	0.435	0.1835	2.92	1055.8	2.217	6.61	476.2	527.9
22	0.025	0.435	0.2029	2.94	1063.0	2.217	6.61	479.5	524.7
23	0.025	0.435	0.1219	2.94	1063.0	2.217	6.61	479.5	517.9
24	0.025	0.435	0.1623	3.12	1128.1	2.217	6.61	508.9	542.3
25	0.025	0.435	0.1864	3.14	1135.3	2.217	6.61	512.1	538.2
26	0.025	0.435	0.1048	3.16	1142.6	2.217	6.61	515.4	533.8
27	0.025	0.435	0.1908	3.30	1193.2	2.217	6.61	538.2	548.8
28	0.025	0.435	0.1245	3.32	1200.4	2.217	6.61	541.5	542.7
29	0.025	0.435	0.1381	3.34	1207.7	2.217	6.61	544.7	535.4
30	0.025	0.435	0.1226	3.34	1207.7	2.217	6.61	544.7	522.7
31	0.025	0.435	0.1581	3.94	1424.6	2.217	6.61	642.6	596.2

*Values are considered to be overestimated; calculated values were used for calculations.

Table 4. Fracture stress data for DUN500S-6B

[2] DUN500S-6B

No.	Thickness, mm	Diameter, mm	Contact diameter, mm	Load, N	Local fracture stress, MPa	Size effect parameter	Weibull modulus (m)	Fracture stress, MPa	Scale parameter, MPa
1	0.03	0.443	0.1010	2.08	570.4	2.565	5.49	222.4	478.9
2	0.03	0.443	0.1234	2.38	652.6	2.565	5.49	254.5	481.6
3	0.03	0.443	0.1007	2.70	740.4	2.565	5.49	288.7	505.9
4	0.03	0.443	0.0911	2.86	784.2	2.565	5.49	305.8	506.9
5	0.03	0.443	0.1070	3.12	855.5	2.565	5.49	333.6	529.3
6	0.03	0.443	0.1321	3.16	866.5	2.565	5.49	337.9	516.8
7	0.03	0.443	0.1143	3.20	877.5	2.565	5.49	342.1	507.1
8	0.03	0.443	0.0947	3.54	970.7	2.565	5.49	378.5	545.6
9	0.03	0.443	0.1349	3.58	981.7	2.565	5.49	382.8	538.1
10	0.03	0.443	0.1504	3.60	987.2	2.565	5.49	384.9	528.8
11	0.03	0.443	0.1280	3.68	1009.1	2.565	5.49	393.5	529.1
12	0.03	0.443	0.1286	3.74	1025.5	2.565	5.49	399.9	527.1
13	0.03	0.443	0.1073	3.74	1025.5	2.565	5.49	399.9	517.3
14	0.03	0.443	0.1191	3.84	1053.0	2.565	5.49	410.6	521.6
15	0.03	0.443	0.1197	3.88	1063.9	2.565	5.49	414.8	518.1
16	0.03	0.443	0.1807	3.90	1069.4	2.565	5.49	417.0	512.1
17	0.03	0.443	0.1140	3.96	1085.9	2.565	5.49	423.4	511.6
18	0.03	0.443	0.1255	3.98	1091.4	2.565	5.49	425.5	506.1
19	0.03	0.443	0.1235	4.02	1102.3	2.565	5.49	429.8	503.3
20	0.03	0.443	0.1394	4.20	1151.7	2.565	5.49	449.1	517.7
21	0.03	0.443	0.1245	4.30	1179.1	2.565	5.49	459.8	521.9
22	0.03	0.443	0.1140	4.30	1179.1	2.565	5.49	459.8	513.8
23	0.03	0.443	0.1273	4.32	1184.6	2.565	5.49	461.9	508.1
24	0.03	0.443	0.1550	4.38	1201.0	2.565	5.49	468.3	506.9
25	0.03	0.443	0.1369	4.46	1223.0	2.565	5.49	476.9	507.6
26	0.03	0.443	0.1397	4.48	1228.5	2.565	5.49	479.0	501.0
27	0.03	0.443	0.1004	4.50	1233.9	2.565	5.49	481.1	493.9
28	0.03	0.443	0.1299	4.54	1244.9	2.565	5.49	485.4	488.1
29	0.03	0.443	0.1264	4.66	1277.8	2.565	5.49	498.2	489.3
30	0.03	0.443	0.1238	4.82	1321.7	2.565	5.49	515.4	491.7
31	0.03	0.443	0.1458	4.84	1327.2	2.565	5.49	517.5	474.1

Table 5. Fracture stress data for DUN500S-7B

[3] DUN500S-7B

No.	Thickness, mm	Diameter, mm	Contact diameter, mm	Load, N	Local fracture stress, MPa	Size effect parameter	Weibull modulus (m)	Fracture stress, MPa	Scale parameter, MPa
1	0.035	0.431	0.1407	4.00	704.3	1.945	7.25	362.1	642.7
2	0.035	0.431	0.1219	4.16	732.5	1.945	7.25	376.6	606.2
3	0.035	0.431	0.1562	4.32	760.7	1.945	7.25	391.1	593.9
4	0.035	0.431		4.44	781.8	1.945	7.25	402.0	585.3
5	0.035	0.431	0.1893	4.48	788.8	1.945	7.25	405.6	571.3
6	0.035	0.431	0.1572	4.76	838.1	1.945	7.25	430.9	590.5
7	0.035	0.431	0.1340	5.00	880.4	1.945	7.25	452.7	605.7
8	0.035	0.431	0.1375	5.08	894.5	1.945	7.25	459.9	602.6
9	0.035	0.431	0.1432	5.28	929.7	1.945	7.25	478.0	614.6
10	0.035	0.431	0.1493	5.44	957.9	1.945	7.25	492.5	622.4
11	0.035	0.431	0.1521	5.50	968.4	1.945	7.25	497.9	619.2
12	0.035	0.431	0.1343	5.58	982.5	1.945	7.25	505.2	618.9
13	0.035	0.431	0.1381	5.60	986.0	1.945	7.25	507.0	612.4
14	0.035	0.431	0.1295	5.66	996.6	1.945	7.25	512.4	610.7
15	0.035	0.431	0.1350	5.78	1017.7	1.945	7.25	523.3	615.6
16	0.035	0.431	0.1293	5.78	1017.7	1.945	7.25	523.3	608.0
17	0.035	0.431	0.1292	5.78	1017.7	1.945	7.25	523.3	600.7
18	0.035	0.431	0.1492	5.82	1024.8	1.945	7.25	526.9	597.8
19	0.035	0.431	0.1295	5.82	1024.8	1.945	7.25	526.9	590.9
20	0.035	0.431	0.1561	5.84	1028.3	1.945	7.25	528.7	586.2
21	0.035	0.431	0.1235	5.94	1045.9	1.945	7.25	537.8	589.5
22	0.035	0.431	0.1565	6.02	1060.0	1.945	7.25	545.0	590.7
23	0.035	0.431	0.1502	6.02	1060.0	1.945	7.25	545.0	584.0
24	0.035	0.431	0.1661	6.12	1077.6	1.945	7.25	554.0	586.8
25	0.035	0.431	0.1480	6.12	1077.6	1.945	7.25	554.0	579.8
26	0.035	0.431	0.1394	6.14	1081.1	1.945	7.25	555.9	574.5
27	0.035	0.431	0.1575	6.48	1141.0	1.945	7.25	586.6	598.4
28	0.035	0.431	0.1464	6.78	1193.8	1.945	7.25	613.8	617.4
29	0.035	0.431	0.1305	6.92	1218.5	1.945	7.25	626.5	620.5
30	0.035	0.431	0.1568	7.00	1232.6	1.945	7.25	633.7	616.7
31	0.035	0.431	0.1346	7.10	1250.2	1.945	7.25	642.8	612.2
32	0.035	0.431	0.1343	7.16	1260.7	1.945	7.25	648.2	598.9

Table 6. Fracture stress data for AGR-06

[4] AGR-06

No.	Thickness, mm	Diameter, mm	Contact diameter, mm	Load, N	Local fracture stress, MPa	Size effect parameter	Weibull modulus (m)	Fracture stress, MPa	Scale parameter, MPa
1	0.0339	0.425	0.1966	4.58	758.9	2.138	6.22	354.9	689.9
2	0.0339	0.425	0.1439	4.66	772.1	2.138	6.22	361.1	626.3
3	0.0339	0.425	0.2045	4.68	775.4	2.138	6.22	362.7	587.8
4	0.0339	0.425	0.1547	4.74	785.4	2.138	6.22	367.3	566.9
5	0.0339	0.425	0.1464	4.88	808.6	2.138	6.22	378.2	561.5
6	0.0339	0.425	0.1328	4.90	811.9	2.138	6.22	379.7	546.0
7	0.0339	0.425	0.1559	4.94	818.5	2.138	6.22	382.8	535.4
8	0.0339	0.425	0.1343	5.00	828.4	2.138	6.22	387.5	528.8
9	0.0339	0.425	0.1328	5.02	831.8	2.138	6.22	389.0	519.3
10	0.0339	0.425	0.2026	5.38	891.4	2.138	6.22	416.9	545.5
11	0.0339	0.425	0.1458	5.44	901.3	2.138	6.22	421.6	541.4
12	0.0339	0.425	0.1254	5.70	944.4	2.138	6.22	441.7	557.4
13	0.0339	0.425	0.1791	5.84	967.6	2.138	6.22	452.6	561.8
14	0.0339	0.425		5.98	990.8	2.138	6.22	463.4	566.3
15	0.0339	0.425	0.1671	6.10	1010.7	2.138	6.22	472.7	569.1
16	0.0339	0.425	0.1591	6.10	1010.7	2.138	6.22	472.7	560.9
17	0.0339	0.425	0.1632	6.22	1030.6	2.138	6.22	482.0	563.9
18	0.0339	0.425	0.1436	6.22	1030.6	2.138	6.22	482.0	556.2
19	0.0339	0.425	0.1213	6.34	1050.5	2.138	6.22	491.3	559.4
20	0.0339	0.425	0.1575	6.38	1057.1	2.138	6.22	494.4	555.4
21	0.0339	0.425	0.1546	6.66	1103.5	2.138	6.22	516.1	572.2
22	0.0339	0.425	0.1359	6.74	1116.7	2.138	6.22	522.3	571.4
23	0.0339	0.425	0.1474	6.78	1123.4	2.138	6.22	525.4	567.2
24	0.0339	0.425	0.1419	6.94	1149.9	2.138	6.22	537.8	572.7
25	0.0339	0.425	0.1480	6.96	1153.2	2.138	6.22	539.4	566.4
26	0.0339	0.425	0.1496	7.14	1183.0	2.138	6.22	553.3	572.7
27	0.0339	0.425	0.1461	7.24	1199.6	2.138	6.22	561.1	572.0
28	0.0339	0.425	0.1677	7.34	1216.1	2.138	6.22	568.8	570.5
29	0.0339	0.425	0.1340	7.38	1222.8	2.138	6.22	571.9	563.4
30	0.0339	0.425	0.1553	7.46	1236.0	2.138	6.22	578.1	557.9
31	0.0339	0.425	0.2569	8.22	1361.9	2.138	6.22	637.0	599.5
32	0.0339	0.425	0.1813	8.32	1378.5	2.138	6.22	644.8	585.6

Table 7. Fracture stress data for AGR-10

[5] AGR-10

No.	Thickness, mm	Diameter, mm	Contact diameter, mm	Load, N	Local fracture stress, MPa	Size effect parameter	Weibull modulus (m)	Fracture stress, MPa	Scale parameter, MPa
1	0.0268	0.359	0.1432	3.12	943.5	2.159	6.40	437.0	799.5
2	0.0268	0.359		3.14	949.6	2.159	6.40	439.8	720.4
3	0.0268	0.359	0.1070	3.16	955.6	2.159	6.40	442.6	678.9
4	0.0268	0.359		3.16	955.6	2.159	6.40	442.6	647.5
5	0.0268	0.359		3.20	967.7	2.159	6.40	448.2	631.7
6	0.0268	0.359	0.0524	3.24	979.8	2.159	6.40	453.9	620.0
7	0.0268	0.359	0.1004	3.32	1004.0	2.159	6.40	465.1	618.6
8	0.0268	0.359	0.1305	3.40	1028.2	2.159	6.40	476.3	618.7
9	0.0268	0.359	0.0959	3.52	1064.5	2.159	6.40	493.1	627.1
10	0.0268	0.359	0.1118	3.58	1082.6	2.159	6.40	501.5	625.6
11	0.0268	0.359	0.1464	3.62	1094.7	2.159	6.40	507.1	621.3
12	0.0268	0.359	0.1134	3.64	1100.8	2.159	6.40	509.9	614.4
13	0.0268	0.359	0.1086	3.64	1100.8	2.159	6.40	509.9	604.9
14	0.0268	0.359	0.1120	3.74	1131.0	2.159	6.40	523.9	612.3
15	0.0268	0.359	0.1019	3.78	1143.1	2.159	6.40	529.5	610.1
16	0.0268	0.359	0.1077	3.94	1191.5	2.159	6.40	551.9	627.2
17	0.0268	0.359	0.1845	4.06	1227.8	2.159	6.40	568.7	637.8
18	0.0268	0.359	0.1127	4.18	1264.1	2.159	6.40	585.5	648.3
19	0.0268	0.359	0.1315	4.20	1270.1	2.159	6.40	588.3	643.2
20	0.0268	0.359	0.1251	4.22	1276.2	2.159	6.40	591.1	638.4
21	0.0268	0.359	0.1032	4.22	1276.2	2.159	6.40	591.1	630.6
22	0.0268	0.359	0.0953	4.28	1294.3	2.159	6.40	599.5	631.8
23	0.0268	0.359		4.28	1294.3	2.159	6.40	599.5	624.2
24	0.0268	0.359	0.1165	4.34	1312.4	2.159	6.40	607.9	625.3
25	0.0268	0.359	0.1166	4.56	1379.0	2.159	6.40	638.7	648.9
26	0.0268	0.359	0.1108	4.66	1409.2	2.159	6.40	652.8	654.8
27	0.0268	0.359	0.1197	4.70	1421.3	2.159	6.40	658.4	651.9
28	0.0268	0.359		4.80	1451.6	2.159	6.40	672.4	656.9
29	0.0268	0.359	0.1340	4.84	1463.7	2.159	6.40	678.0	652.9
30	0.0268	0.359		4.94	1493.9	2.159	6.40	692.0	656.3
31	0.0268	0.359		5.06	1530.2	2.159	6.40	708.8	660.9
32	0.0268	0.359	0.1381	5.20	1572.5	2.159	6.40	728.4	666.1
33	0.0268	0.359	0.1235	5.24	1584.6	2.159	6.40	734.0	655.4
34	0.0268	0.359	0.1242	5.54	1675.3	2.159	6.40	776.0	669.9

Table 8. Fracture stress data for LEU01-46T

[6] LEU01-46T

No.	Thickness, mm	Diameter, mm	Contact diameter, mm	Load, N	Local fracture stress, MPa	Size effect parameter	Weibull modulus (m)	Fracture stress, MPa	Scale parameter, MPa
1	0.0353	0.3795	0.1213	6.24	794.5	3.015	3.98	263.5	698.6
2	0.0353	0.3795	0.1486	6.36	809.8	3.015	3.98	268.6	595.8
3	0.0353	0.3795	0.1524	6.60	840.3	3.015	3.98	278.7	556.1
4	0.0353	0.3795	0.1321	6.82	868.3	3.015	3.98	288.0	532.3
5	0.0353	0.3795	0.1559	6.92	881.1	3.015	3.98	292.2	508.5
6	0.0353	0.3795	0.1321	6.96	886.2	3.015	3.98	293.9	486.3
7	0.0353	0.3795	0.1378	7.02	893.8	3.015	3.98	296.4	469.7
8	0.0353	0.3795	0.1346	7.44	947.3	3.015	3.98	314.2	479.1
9	0.0353	0.3795	0.1607	7.56	962.6	3.015	3.98	319.2	470.4
10	0.0353	0.3795		7.96	1013.5	3.015	3.98	336.1	479.9
11	0.0353	0.3795	0.1610	8.12	1033.9	3.015	3.98	342.9	475.4
12	0.0353	0.3795	0.1530	8.22	1046.6	3.015	3.98	347.1	468.3
13	0.0353	0.3795	0.1581	8.30	1056.8	3.015	3.98	350.5	460.8
14	0.0353	0.3795	0.1676	8.40	1069.5	3.015	3.98	354.7	455.1
15	0.0353	0.3795	0.1387	8.42	1072.1	3.015	3.98	355.5	445.6
16	0.0353	0.3795	0.1515	8.52	1084.8	3.015	3.98	359.8	440.8
17	0.0353	0.3795	0.1753	8.56	1089.9	3.015	3.98	361.5	433.2
18	0.0353	0.3795	0.1483	8.80	1120.4	3.015	3.98	371.6	435.9
19	0.0353	0.3795	0.1480	8.94	1138.3	3.015	3.98	377.5	433.6
20	0.0353	0.3795	0.1505	9.06	1153.6	3.015	3.98	382.6	430.4
21	0.0353	0.3795	0.1794	9.46	1204.5	3.015	3.98	399.5	440.1
22	0.0353	0.3795		10.02	1275.8	3.015	3.98	423.1	456.6
23	0.0353	0.3795	0.1457	10.14	1291.1	3.015	3.98	428.2	452.5
24	0.0353	0.3795	0.1330	10.50	1336.9	3.015	3.98	443.4	458.7
25	0.0353	0.3795	0.1509	11.02	1403.1	3.015	3.98	465.3	471.1
26	0.0353	0.3795	0.1702	11.28	1436.2	3.015	3.98	476.3	471.4
27	0.0353	0.3795	0.1600	11.58	1474.4	3.015	3.98	489.0	472.5
28	0.0353	0.3795		12.40	1578.8	3.015	3.98	523.6	493.2
29	0.0353	0.3795	0.1639	14.70	1871.7	3.015	3.98	620.7	568.5
30	0.0353	0.3795	0.1816	15.34	1953.1	3.015	3.98	647.7	574.5
31	0.0353	0.3795	0.1508	15.34	1953.1	3.015	3.98	647.7	552.4
32	0.0353	0.3795	0.1511	15.42	1963.3	3.015	3.98	651.1	525.3

Table 9. Fracture stress data for LEU01-49T

[7] LEU01-49T

No.	Thickness, mm	Diameter, mm	Contact diameter, mm	Load, N	Local fracture stress, MPa	Size effect parameter	Weibull modulus (m)	Fracture stress, MPa	Scale parameter, MPa
1	0.0359	0.378	0.1238	5.42	830.7	2.048	6.35	405.6	756.1
2	0.0359	0.378	0.1277	6.18	947.2	2.048	6.35	462.5	771.2
3	0.0359	0.378	0.1327	6.74	1033.0	2.048	6.35	504.4	787.2
4	0.0359	0.378	0.1346	6.78	1039.2	2.048	6.35	507.4	755.0
5	0.0359	0.378	0.1429	6.96	1066.8	2.048	6.35	520.8	746.5
6	0.0359	0.378	0.1457	7.20	1103.5	2.048	6.35	538.8	748.5
7	0.0359	0.378	0.1416	7.38	1131.1	2.048	6.35	552.2	746.8
8	0.0359	0.378	0.1286	7.54	1155.7	2.048	6.35	564.2	745.2
9	0.0359	0.378	0.1489	7.64	1171.0	2.048	6.35	571.7	739.2
10	0.0359	0.378	0.1343	7.80	1195.5	2.048	6.35	583.7	740.1
11	0.0359	0.378	0.1451	7.90	1210.8	2.048	6.35	591.2	736.3
12	0.0359	0.378	0.1515	7.96	1220.0	2.048	6.35	595.7	729.6
13	0.0359	0.378	0.1369	8.08	1238.4	2.048	6.35	604.6	729.0
14	0.0359	0.378	0.1438	8.14	1247.6	2.048	6.35	609.1	723.6
15	0.0359	0.378	0.1375	8.26	1266.0	2.048	6.35	618.1	723.9
16	0.0359	0.378	0.1461	8.32	1275.2	2.048	6.35	622.6	719.3
17	0.0359	0.378	0.1302	8.36	1281.3	2.048	6.35	625.6	713.3
18	0.0359	0.378	0.1445	8.38	1284.4	2.048	6.35	627.1	705.9
19	0.0359	0.378	0.1543	8.56	1312.0	2.048	6.35	640.5	712.1
20	0.0359	0.378	0.1401	8.64	1324.3	2.048	6.35	646.5	710.0
21	0.0359	0.378	0.1600	9.04	1385.6	2.048	6.35	676.5	734.0
22	0.0359	0.378		9.04	1385.6	2.048	6.35	676.5	725.3
23	0.0359	0.378	0.1267	9.10	1394.8	2.048	6.35	681.0	721.5
24	0.0359	0.378	0.1343	9.12	1397.8	2.048	6.35	682.5	714.5
25	0.0359	0.378	0.1397	9.36	1434.6	2.048	6.35	700.4	724.5
26	0.0359	0.378	0.1582	9.38	1437.7	2.048	6.35	701.9	717.3
27	0.0359	0.378	0.1407	9.38	1437.7	2.048	6.35	701.9	708.4
28	0.0359	0.378	0.1407	9.50	1456.1	2.048	6.35	710.9	708.3
29	0.0359	0.378	0.1476	9.64	1477.5	2.048	6.35	721.4	709.2
30	0.0359	0.378	0.1470	10.18	1560.3	2.048	6.35	761.8	738.4
31	0.0359	0.378	0.1483	10.28	1575.6	2.048	6.35	769.3	734.3
32	0.0359	0.378	0.1591	11.00	1686.0	2.048	6.35	823.1	772.6
33	0.0359	0.378	0.1438	11.06	1695.2	2.048	6.35	827.6	761.9
34	0.0359	0.378	0.1550	11.60	1777.9	2.048	6.35	868.0	780.3
35	0.0359	0.378	0.1619	12.46	1909.7	2.048	6.35	932.4	810.3

Table 10. Fracture stress data for B&W-93059

[8] B&W-93059

No.	Thickness, mm	Diameter, mm	Contact diameter, mm	Load, N	Local fracture stress, MPa	Size effect parameter	Weibull modulus (m)	Fracture stress, MPa	Scale parameter, MPa
1	0.0343	0.3985	0.1639	4.74	675.8	1.99	6.58	339.6	631.3
2	0.0343	0.3985	0.1566	4.96	707.2	1.99	6.58	355.4	593.2
3	0.0343	0.3985	0.1457	4.98	710.0	1.99	6.58	356.8	558.8
4	0.0343	0.3985	0.1312	5.30	755.6	1.99	6.58	379.7	568.0
5	0.0343	0.3985	0.1566	5.32	758.5	1.99	6.58	381.2	549.8
6	0.0343	0.3985	0.1559	5.34	761.3	1.99	6.58	382.6	535.5
7	0.0343	0.3985	0.1362	5.38	767.0	1.99	6.58	385.5	525.7
8	0.0343	0.3985	0.1521	5.40	769.9	1.99	6.58	386.9	515.7
9	0.0343	0.3985	0.1642	5.50	784.1	1.99	6.58	394.1	514.6
10	0.0343	0.3985	0.1546	5.56	792.7	1.99	6.58	398.4	510.6
11	0.0343	0.3985	0.1451	5.70	812.7	1.99	6.58	408.4	514.4
12	0.0343	0.3985	0.1422	5.80	826.9	1.99	6.58	415.6	515.1
13	0.0343	0.3985	0.1359	5.80	826.9	1.99	6.58	415.6	507.3
14	0.0343	0.3985	0.1594	5.86	835.5	1.99	6.58	419.9	505.3
15	0.0343	0.3985	0.1575	5.92	844.0	1.99	6.58	424.2	503.5
16	0.0343	0.3985	0.1616	6.06	864.0	1.99	6.58	434.2	508.7
17	0.0343	0.3985	0.1524	6.36	906.8	1.99	6.58	455.7	527.1
18	0.0343	0.3985	0.1499	6.52	929.6	1.99	6.58	467.1	533.7
19	0.0343	0.3985	0.1696	6.60	941.0	1.99	6.58	472.9	533.8
20	0.0343	0.3985	0.1375	6.66	949.5	1.99	6.58	477.2	532.3
21	0.0343	0.3985	0.1442	6.68	952.4	1.99	6.58	478.6	527.8
22	0.0343	0.3985	0.1778	6.70	955.2	1.99	6.58	480.0	523.3
23	0.0343	0.3985	0.1607	6.82	972.3	1.99	6.58	488.6	526.6
24	0.0343	0.3985	0.1667	7.00	998.0	1.99	6.58	501.5	534.3
25	0.0343	0.3985	0.1616	7.22	1029.4	1.99	6.58	517.3	544.7
26	0.0343	0.3985	0.1375	7.26	1035.1	1.99	6.58	520.2	541.4
27	0.0343	0.3985	0.1467	7.28	1037.9	1.99	6.58	521.6	536.4
28	0.0343	0.3985	0.1426	7.30	1040.8	1.99	6.58	523.0	531.2
29	0.0343	0.3985	0.1607	7.68	1094.9	1.99	6.58	550.3	551.7
30	0.0343	0.3985	0.1762	7.70	1097.8	1.99	6.58	551.7	545.6
31	0.0343	0.3985	0.1556	7.72	1100.6	1.99	6.58	553.1	539.0
32	0.0343	0.3985	0.1778	7.84	1117.8	1.99	6.58	561.7	538.6
33	0.0343	0.3985	0.1521	8.16	1163.4	1.99	6.58	584.6	550.2
34	0.0343	0.3985	0.1508	8.72	1243.2	1.99	6.58	624.8	574.6
35	0.0343	0.3985	0.1553	8.78	1251.8	1.99	6.58	629.1	560.0

Table 11. Fracture stress data for B&W-93060

[9] B&W-93060

No.	Thickness, mm	Diameter, mm	Contact diameter, mm	Load, N	Local fracture stress, MPa	Size effect parameter	Weibull modulus (m)	Fracture stress, MPa	Scale parameter, MPa
1	0.0368	0.4065	0.1223	3.74	406.4	2.333	5.15	174.2	380.3
2	0.0368	0.4065	0.1527	4.34	471.6	2.333	5.15	202.2	384.6
3	0.0368	0.4065		4.86	528.2	2.333	5.15	226.4	396.8
4	0.0368	0.4065	0.1721	5.16	560.8	2.333	5.15	240.4	397.1
5	0.0368	0.4065	0.1657	5.70	619.4	2.333	5.15	265.5	418.7
6	0.0368	0.4065	0.1588	5.88	639.0	2.333	5.15	273.9	415.5
7	0.0368	0.4065		6.04	656.4	2.333	5.15	281.4	412.8
8	0.0368	0.4065	0.1810	6.04	656.4	2.333	5.15	281.4	400.7
9	0.0368	0.4065	0.1642	6.26	680.3	2.333	5.15	291.6	404.4
10	0.0368	0.4065	0.1781	6.58	715.1	2.333	5.15	306.5	414.9
11	0.0368	0.4065	0.1464	6.66	723.8	2.333	5.15	310.3	410.6
12	0.0368	0.4065	0.1556	6.70	728.1	2.333	5.15	312.1	404.4
13	0.0368	0.4065	0.1495	6.72	730.3	2.333	5.15	313.1	397.6
14	0.0368	0.4065	0.1721	6.84	743.3	2.333	5.15	318.7	397.1
15	0.0368	0.4065	0.1689	6.94	754.2	2.333	5.15	323.3	395.7
16	0.0368	0.4065	0.1651	7.12	773.8	2.333	5.15	331.7	398.9
17	0.0368	0.4065	0.1867	7.26	789.0	2.333	5.15	338.2	399.9
18	0.0368	0.4065	0.1553	7.38	802.0	2.333	5.15	343.8	399.9
19	0.0368	0.4065	0.1512	7.42	806.4	2.333	5.15	345.7	395.5
20	0.0368	0.4065	0.1626	7.44	808.5	2.333	5.15	346.6	390.3
21	0.0368	0.4065	0.1721	7.56	821.6	2.333	5.15	352.2	390.3
22	0.0368	0.4065	0.1763	7.60	825.9	2.333	5.15	354.1	386.1
23	0.0368	0.4065	0.1639	7.76	843.3	2.333	5.15	361.5	387.9
24	0.0368	0.4065	0.1721	7.96	865.0	2.333	5.15	370.8	391.4
25	0.0368	0.4065	0.1727	8.16	886.8	2.333	5.15	380.2	394.6
26	0.0368	0.4065	0.1728	8.26	897.6	2.333	5.15	384.8	392.5
27	0.0368	0.4065	0.1550	8.36	908.5	2.333	5.15	389.5	390.0
28	0.0368	0.4065	0.1584	8.44	917.2	2.333	5.15	393.2	386.0
29	0.0368	0.4065	0.1772	8.76	952.0	2.333	5.15	408.1	392.1
30	0.0368	0.4065	0.1743	9.24	1004.1	2.333	5.15	430.5	403.4
31	0.0368	0.4065	0.1667	9.66	1049.8	2.333	5.15	450.0	409.2

Appendix A: SiC microstructure of samples used in this study

DUN500S-14B 1340°C Ar/H mix

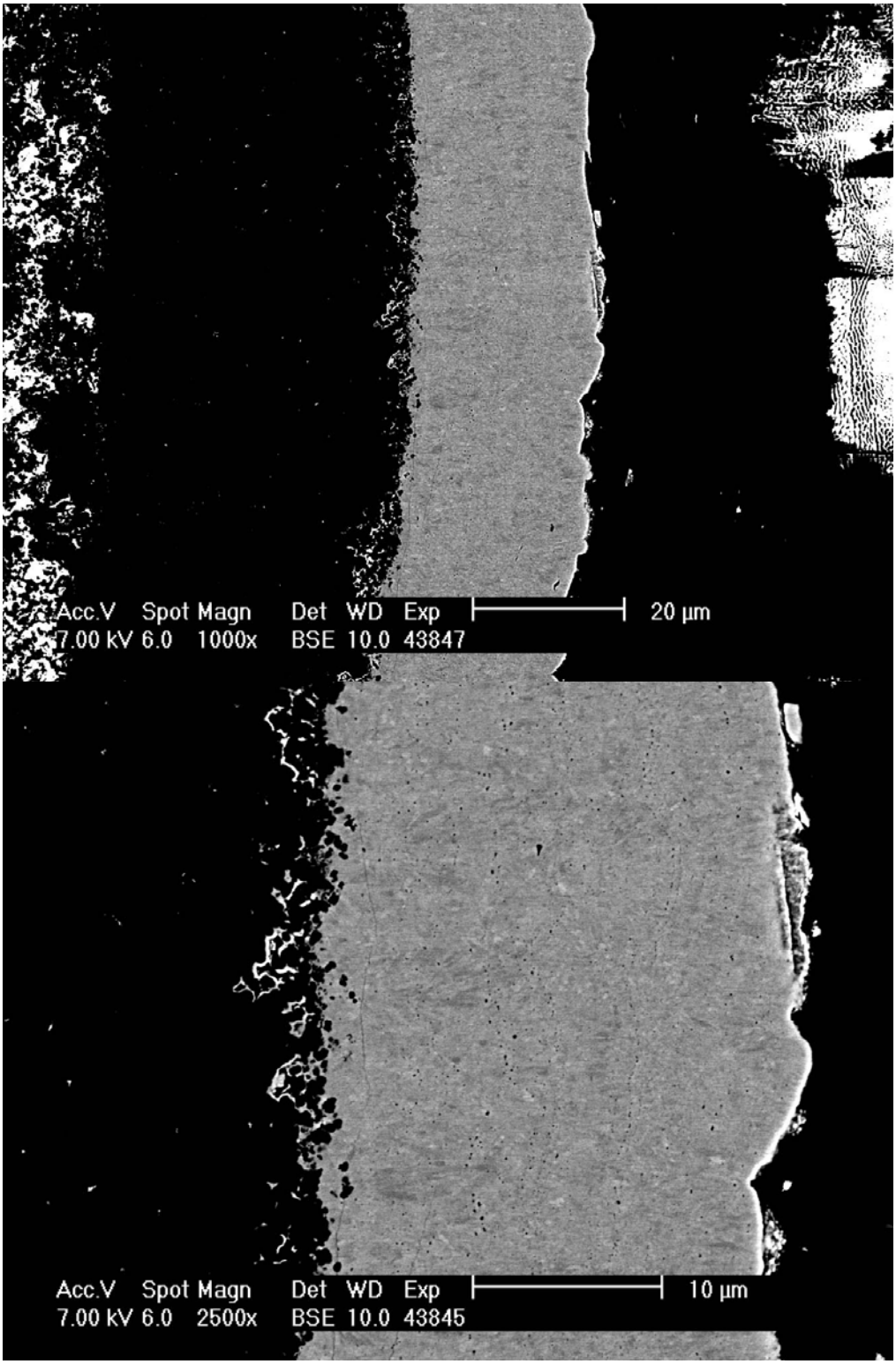

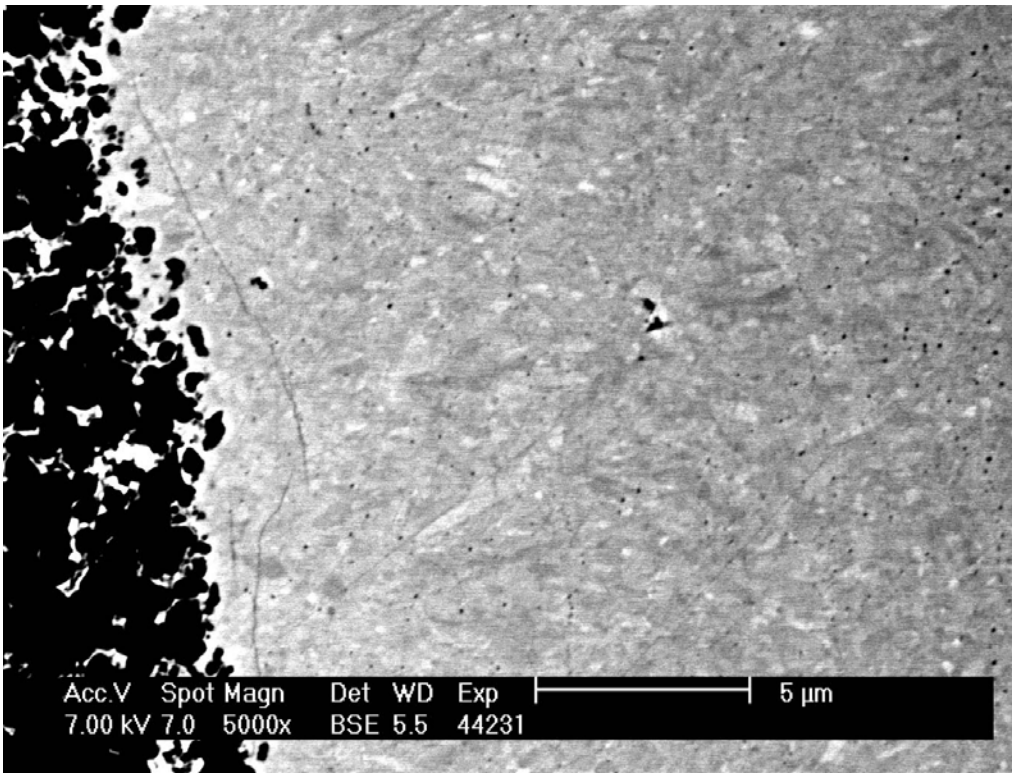
Acc.V Spot Magn Det WD Exp
7.00 kV 7.0 5000x BSE 5.5 44231
5 µm

DUN500S-6B 1510°C H only

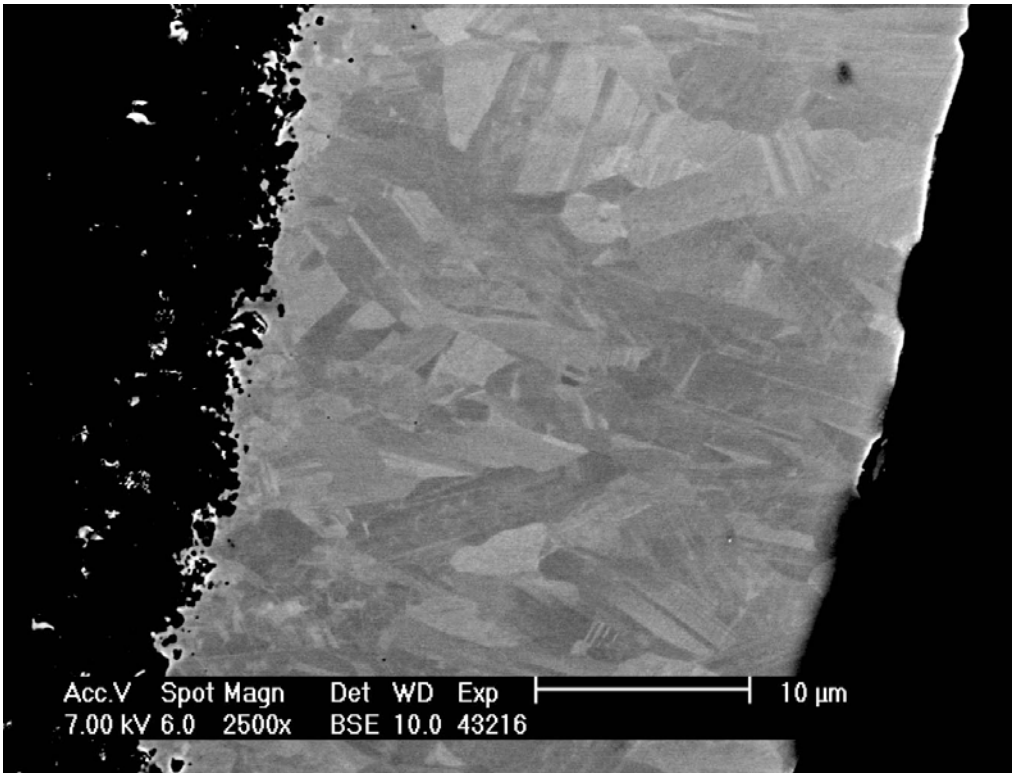

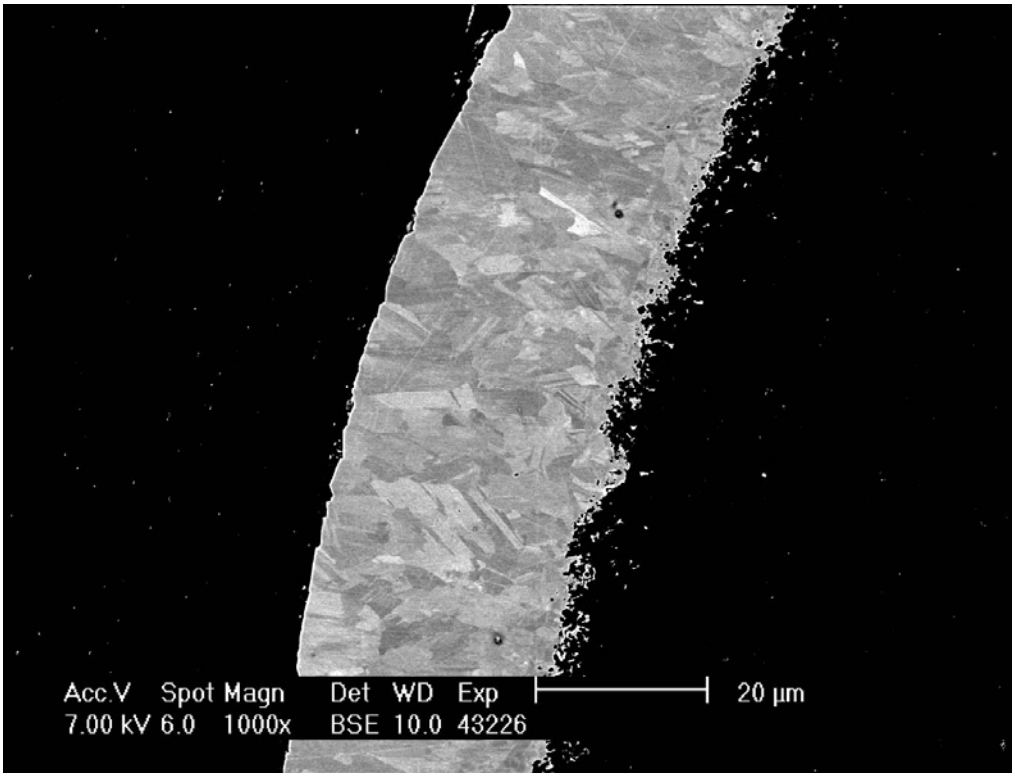

DUN500-7B 1440°C Ar/H mix

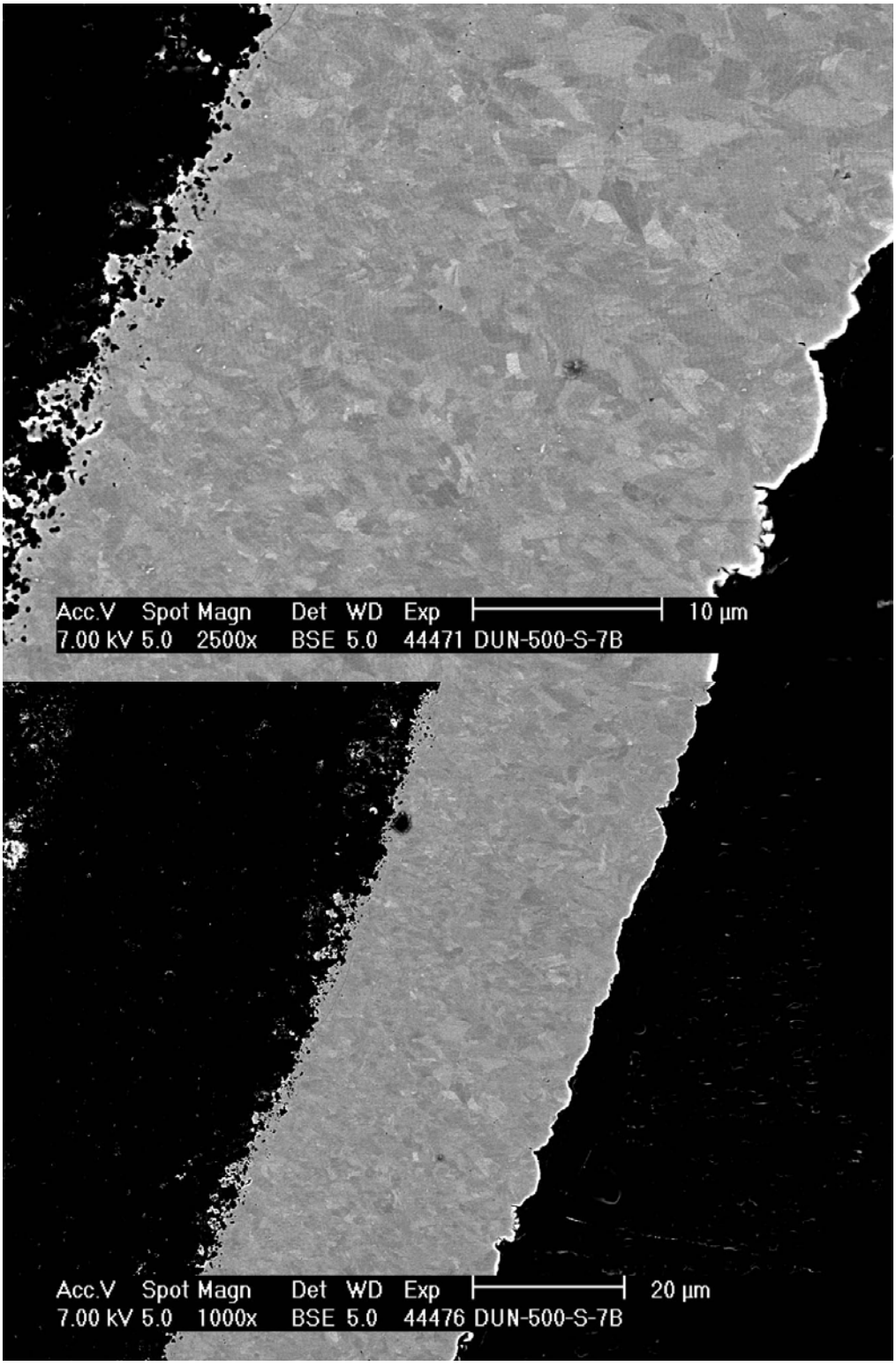

AGR-06 German Reference Fuel

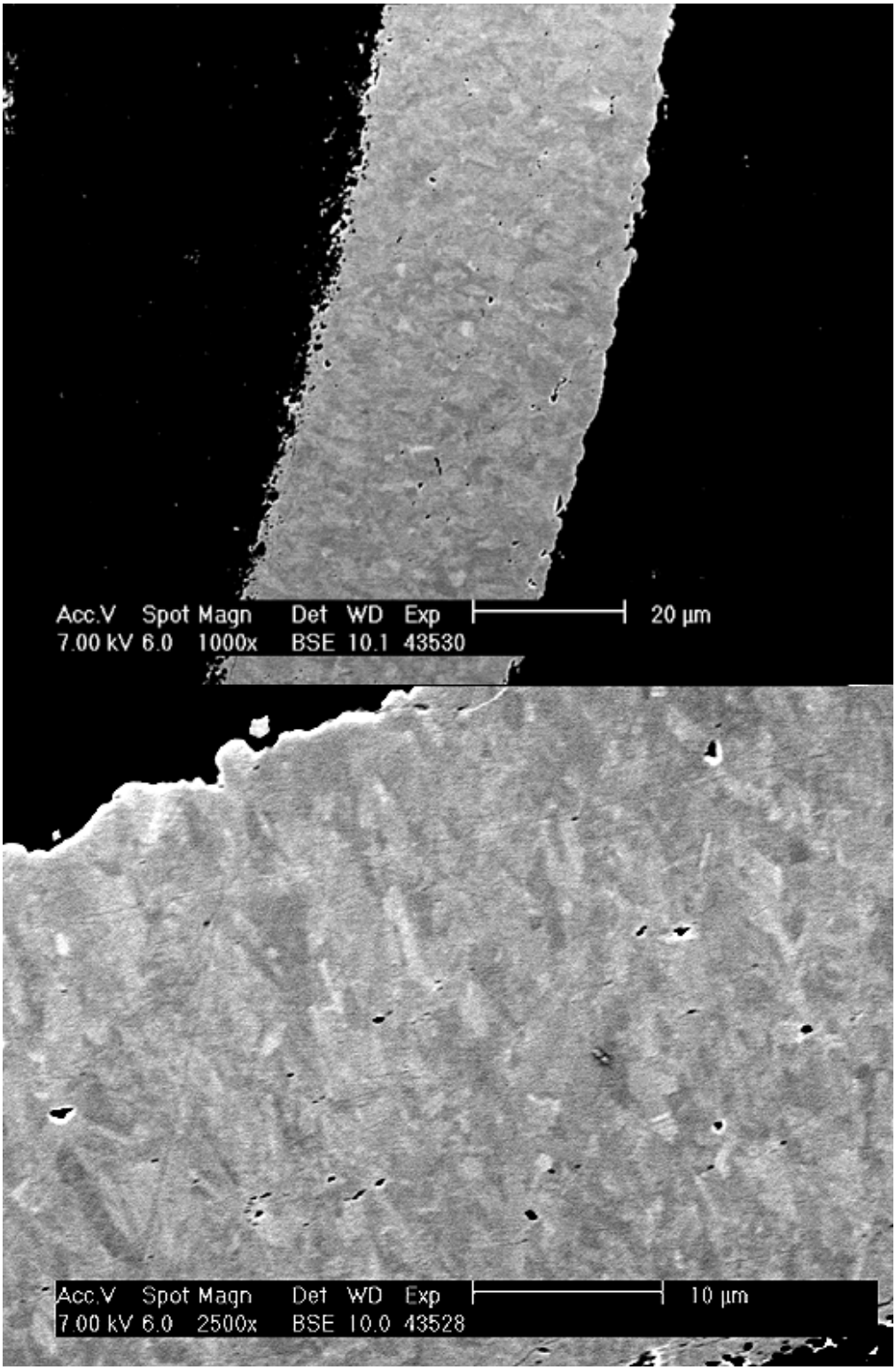

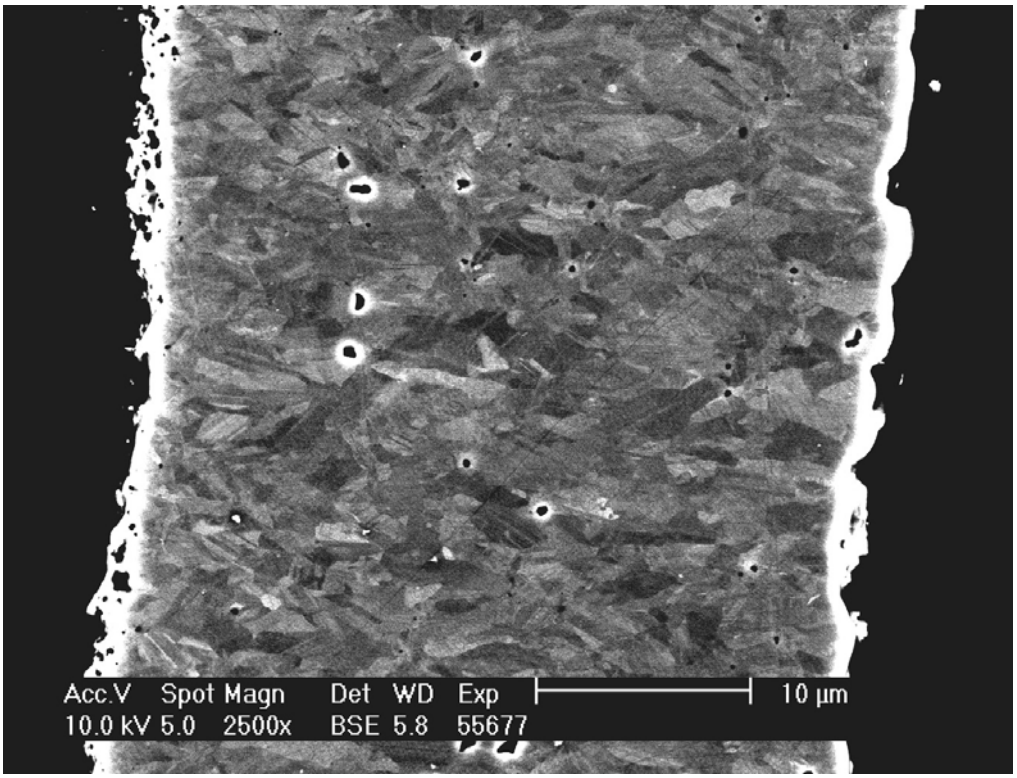
Acc.V Spot Magn Det WD Exp
10.0 kV 5.0 2500x BSE 5.8 55677
10 µm

AGR-10 HRB-21 reference fuel

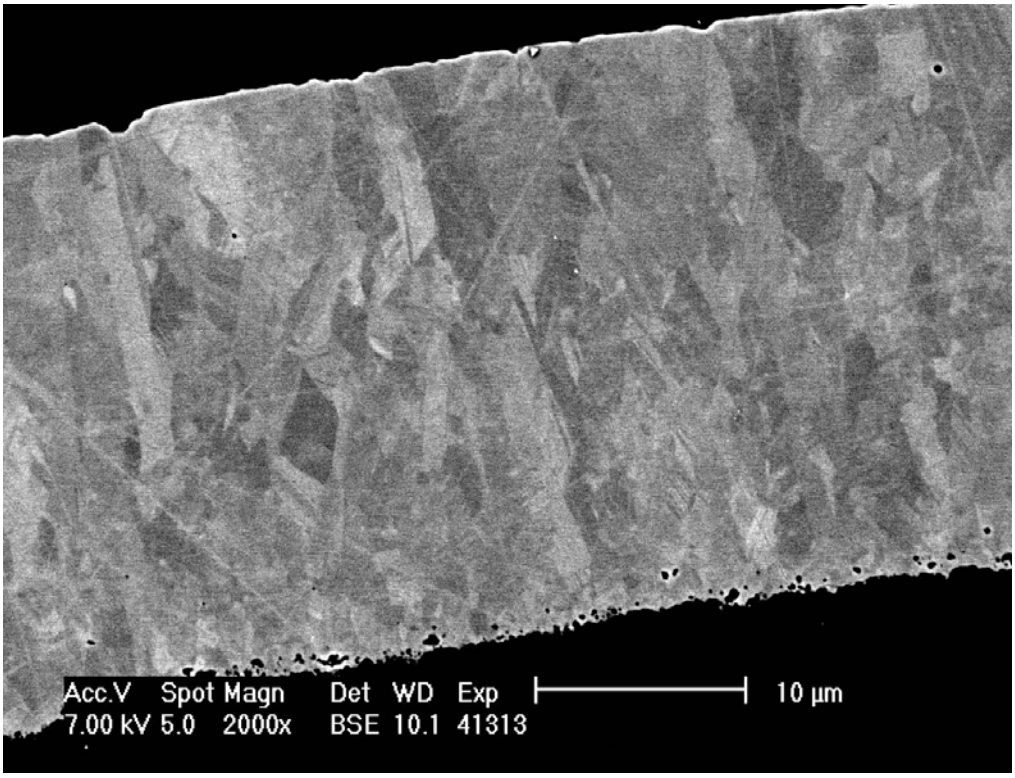

LEU01-46T AGR-1 Baseline

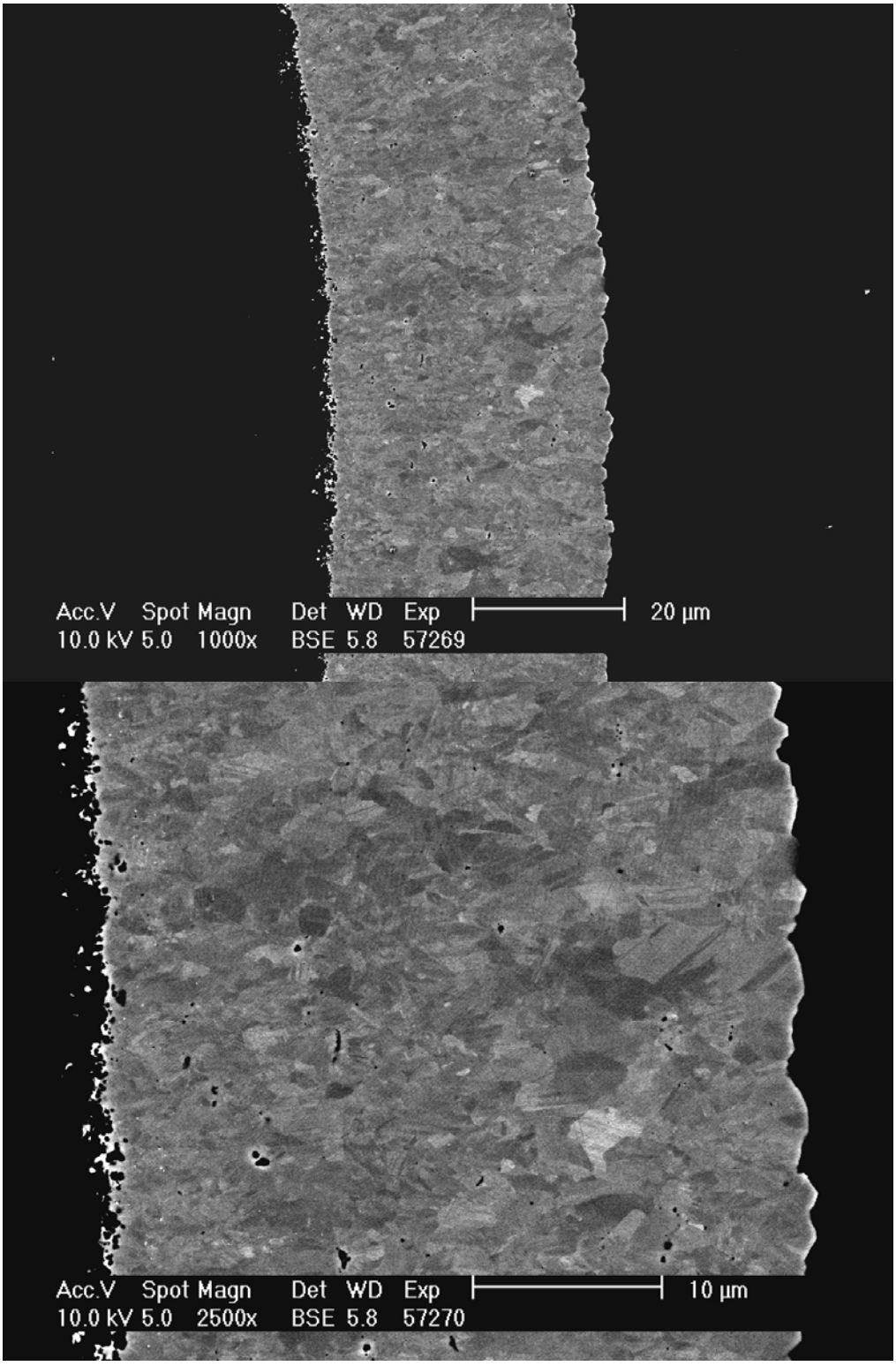

LEU01-49T AGR-1 Variant 3

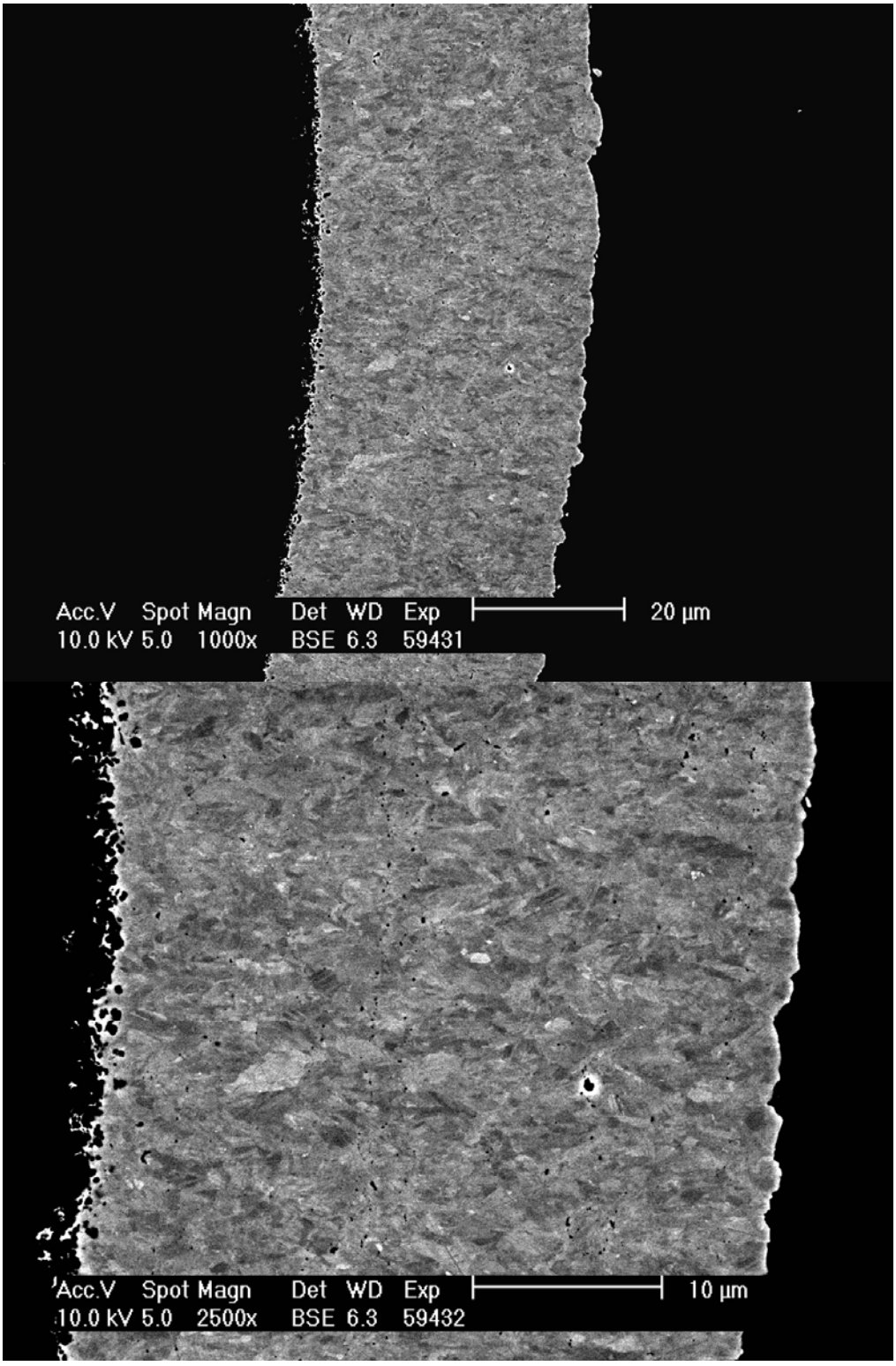

B&W-93059 AGR-2 Variant 1 Qualification Batch

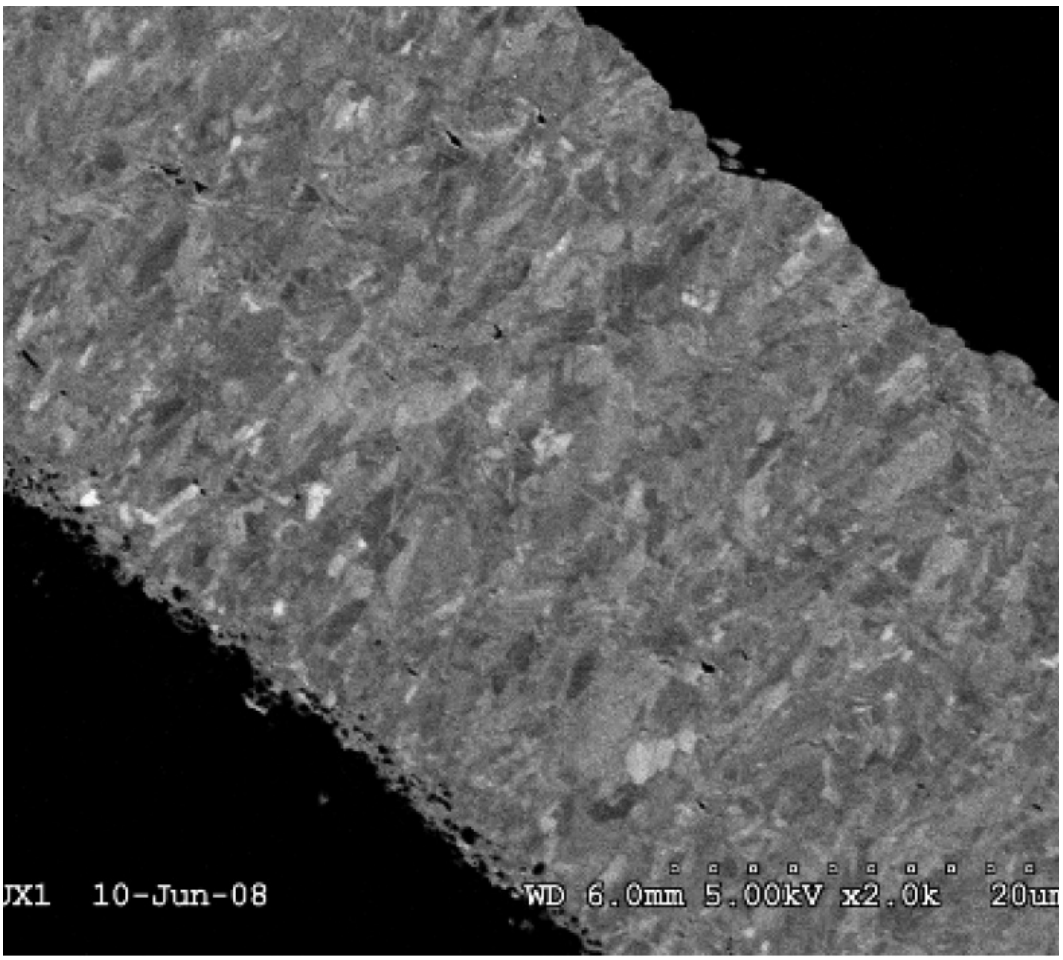

(Image taken from July 2008 NGNP Monthly report, document ID INL/EXT-07-13532.)

B&W-93060 AGR-2 Baseline Qualification Batch

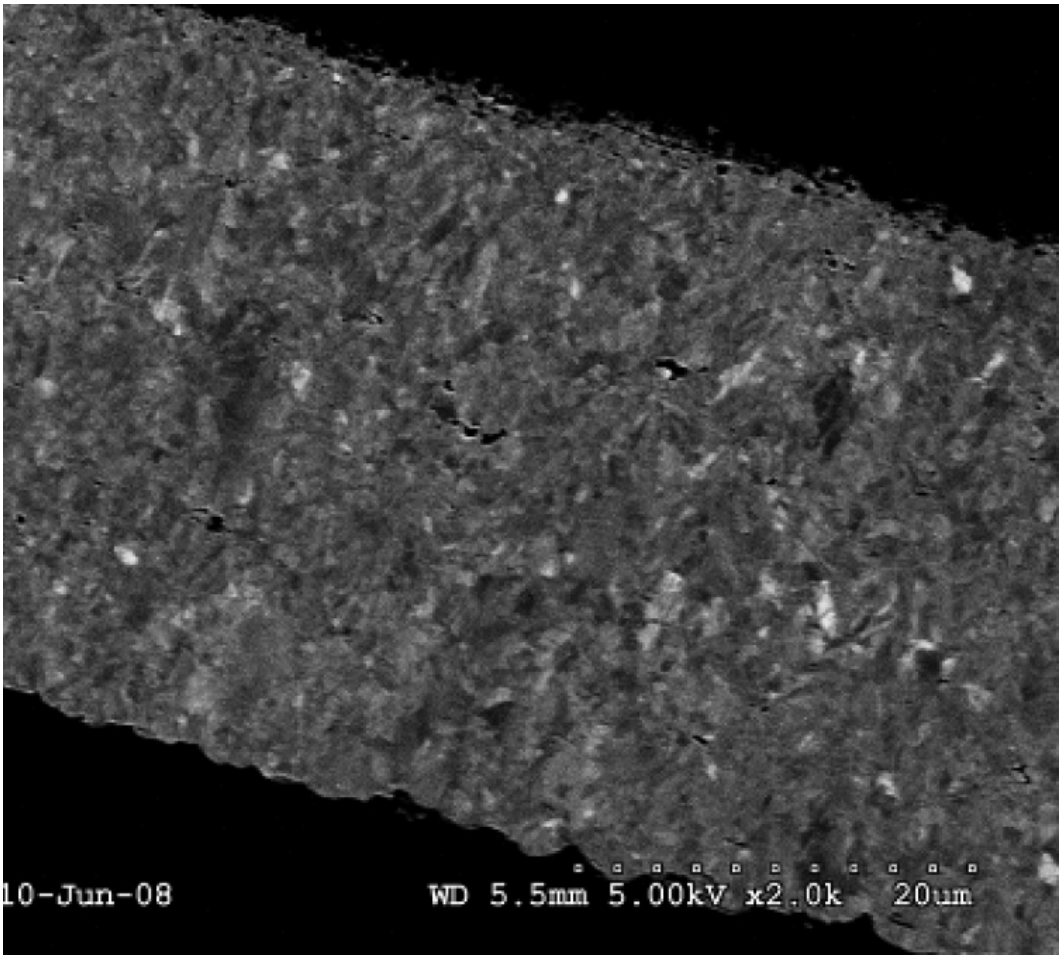

(Image taken from July 2008 NGNP Monthly report , document ID INL/EXT-07-13532.)